Progr Colloid Polym Sci (2000) 115: 59–65

A. Stipp
C. Sinn
T. Palberg
I. Weber
E. Bartsch

Crystallizing polystyrene microgel colloids

A. Stipp (✉) · C. Sinn · T. Palberg
Johannes-Gutenberg-Universität
Institut für Physik, Staudingerweg 7
55099 Mainz, Germany
e-mail: andreas.stipp@uni-mainz.de
Tel.: +49-6131-3923636
Fax: +49-6131-3922991

I. Weber · E. Bartsch
Johannes-Gutenberg-Universität
Institut für physikalische Chemie
Jakob-Welder-Weg 11
55099 Mainz, Germany

Abstract Spherical microgel particles of sufficiently high degree of internal cross-linking and swollen in a good solvent in many respects behave quite similarly to hard-sphere colloids. Due to solvent uptake they can be refractive-index-matched and density-matched in suitable organic solvents. We present preliminary measurements of the crystallization kinetics of 1:10 cross-linked polystyrene microgel particles. We measured Bragg and small-angle light scattering of the solidifying shear melt. Two different scattering patterns, a set of Debye–Scherrer rings and a second ring pattern at small angles could be observed. We check for similarities and differences compared to previously investigated colloidal systems.

Key words Colloidal suspensions · Microgel particles · Hard spheres · Crystallization kinetics · Light scattering

Introduction

Colloidal suspensions of spherical particles with hard-sphere (HS)-like interactions have become a well-recognized experimental model system of soft condensed matter physics over the last few years. A large body of work has been carried out on systems of poly(methyl methacrylate) (PMMA) particles [1] and silica particles [2] in organic solvents and their structural and dynamic properties have been comprehensively studied. Another important aspect was their phase behaviour and the formation of crystalline long-ranged order under certain conditions [3]. The HS system shows a first-order freezing transition (the freezing point) at a volume fraction φ_f of 0.494; above the melting point (φ_m = 0.545) the sample is fully crystallized [4]. In-between fluid and crystal coexist. Also the kinetics of the crystallization kinetics has been investigated extensively and with various techniques [5, 6]. For example, Harland et al. [7] used Bragg light scattering (BLS) to monitor the temporal evolution of the crystal order on the length scale of inter particle distances. Small-angle light scattering (SALS) detects long-ranged density fluctuations, such as growing crystals with surrounding depletion zones and remaining fluid [8, 9]. From both, nucleation rates, growth velocities and crystal densities were extracted and analysed in terms of classical nucleation and growth theories [7, 9, 10].

Microgel particles, also known as micronetwork particles, on the other hand are spherical networks of cross-linked polymer chains which are swollen in a good solvent. They may be synthesized with high average cross-link density, which guarantees that free polymer chains on the particle surface are very short relative to the particle radius, R. Second, the volume swelling ratio, $S = R^3_{\text{swollen}}/R^3_{\text{unswollen}}$, can be tuned to be very small and then elastic deformation of the particles at high volume fractions can be avoided. Recent investigations show that under these conditions microgel particles may be regarded as well-defined model suspensions with HS-like potential [11, 12]. In addition, however, due to solvent uptake they can be density- (and index-) matched in suitable organic solvents; thus, sedimentation effects can be either introduced or avoided. Further, in principle, they offer the possibility of introducing subtle deviations from a pure HS interaction potential. In fact, for a smaller cross-link density,

deviations towards more soft-sphere-like behaviour are clearly detectable [13, 14].

For these reasons there has been growing interest in the behaviour of microgel particles compared to the HS reference system. Up to now mainly states of short-range order both below and above the glass transition (located at $\varphi_f \approx 0.58$) have been investigated. There structural and diffusive data of highly cross-linked samples were observed to closely follow predictions for HS suspensions [12, 15, 16]. While it is known that monodisperse microgel particles do show crystallization, to the best of our knowledge, no measurements of the kinetics of solidification have been presented so far. Such data would be very desirable to have a further check of HS behaviour.

We here present the first measurements of the crystallization kinetics of a suspension of highly cross-linked microgels. The particles were synthesized and prepared to yield crystallizing systems. Microscopy allowed the selection of a suitable sample. We use combined BLS and SALS experiments to analyse the temporal evolution of crystal sizes and structural details. We observed many features very similar to those known from HS systems but we also observed specific differences.

Experimental

Polystyrene microgel particles were synthesized by surfactant-free emulsion polymerization with the cross-linker diisopropenyl benzene as co-monomer, using $K_2S_2O_8$ as the radical initiator and bidistilled water as the solvent. The average cross-link density was 1:10. Details of the synthesis and the subsequent freeze-drying process can be found elsewhere [17]. The particles were redispersed in 2-ethylnaphthalene (EN), which is an index- and density-matching, good solvent for the microgels.[1]

Samples with different volume fractions were made by filling the desired amount of stock suspension into rectangular light scattering cuvettes with dimensions 10×5 mm^2 and adding weighed amounts of solvent. The particles were left undisturbed for some months to equilibrate the swelling process. In the final state, they consisted of about 50% solvent. Dilute samples were characterized by SLS and dynamic light scattering, from which a particle radius of $R_{\text{swollen}} = 360$ nm and a polydispersity $\sigma \approx 6\%$ resulted.

Volume fractions of the more concentrated samples were calculated from the weight fractions [14] using a swelling ratio of $S = 2.1 \pm 0.1$ [18].[2] As this estimate introduces a nonnegligible uncertainty, the volume fractions given later are referred to as nominal volume fractions.

After equilibration samples of nominal volume fraction, φ, larger than φ_f, showed more or less complete crystallization but no detectable sedimentation effects. Fully crystalline samples recrystallized within roughly 1 day after shear-melting. Thus, their solidification kinetics is conveniently accessible in both the early stage of nucleation and growth and in the later stage of ripening.

Under white light illumination beautiful iridescence indicated the presence of ordered structures with interparticle spacings on a length scale comparable to the wavelength of visible light. We note that not all samples showed a homogeneously crystalline appearance. One of the exceptions is shown in Fig. 1. In this sample of $\varphi = 0.55$, both crystalline regions (as identified by the brilliant opalescence of the crystallites) and noncrystalline regions (showing a continuous rainbowlike change in colours) appeared. The boundary between the two regions was observed to be rather sharp: the reason for this is not yet known, but it possibly originates from a transient "polydispersity" caused by still incomplete swelling. Other samples at volume fractions well above φ with very small crystallites showed regions of preferred orientations as identified by a still specular scattering pattern but a more continuous colour change. These possibly result from the shear-melting process applied before. Similar observations were made on HS and are shown and discussed in Ref. [19].

To avoid artefacts such as structural or orientational inhomogenieties we chose the sample of $\varphi \approx 0.54$, shown in Fig. 2. It shows randomly oriented, homogeneously nucleated crystals over the whole sample volume. After several days the average crystal diameter was about 50–100 μm.

We note the appearance of "streaky" crystals, which indicates twinning. This is also well known from crystals of charged spheres [20]. For PMMA spheres–crystallizing in either face-centred-cubic (fcc) or hexagonal-close-packed lattices–the formation of a twin boundary corresponds to the introduction of a stacking fault [21]. While in our case the number of stacking faults seems to be rather small at late stages, in some HS cases even complete random stacking has been observed [22].

The crystallization process was investigated by BLS and SALS. To avoid parasitic reflections the sample cuvette was placed in an index-matching bath containing EN and the detection optics were chosen to be of similar refractive index. For illumination we used a widened (diameter 8 mm) He-Ne laser beam ($\lambda_0 = 632.8$ nm). This was focused onto the centre of the small-angle detector (distance from sample about 1.5 m). To avoid mechanical disturbances, the sample was fixed and the Bragg detector, which was an array of photodiodes mounted on an arm, was rotated around the optical axis. Thus, either the full two-dimensional scattering pattern or

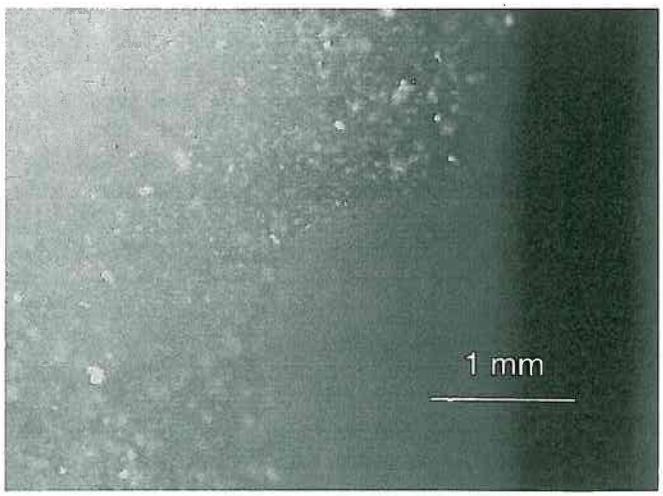

Fig. 1 Incomplete crystallization in a sample of nominal volume fraction of $\varphi = 0.55$. See text for details

[1] $n_D^{PS} = 1.598$, $n_D^{DIPB} = 1.556$, $n_D^{EN} = 1.599$, $\rho^{PS} = 1.05\,\text{g cm}^{-3}$, $\rho^{DIPB} = 0.952\,\text{g cm}^{-3}$, $\rho^{EN} = 0.998\,\text{g cm}^{-3}$ (all values given for ambient temperature).

[2] The complete phase diagram of the particles under study here is not yet available. Therefore we used a similar batch of the same cross-linking density to estimate the swelling ratio leading to typical values of $S = 2.1 \pm 0.1$.

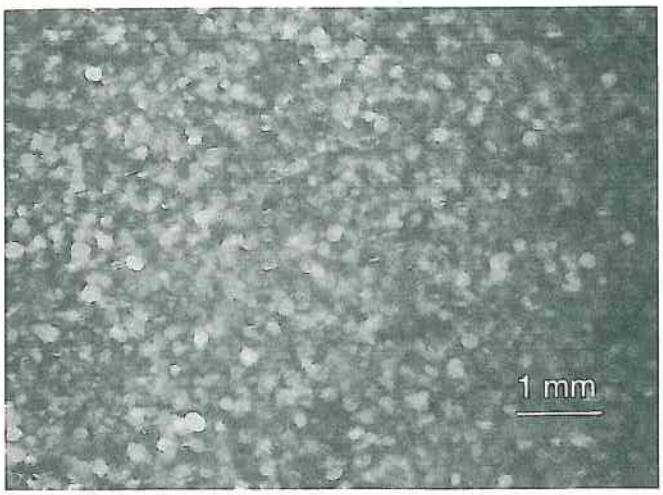

Fig. 2 Complete and homogeneous crystallization in a sample of nominal volume fraction of $\varphi = 0.54$

after angular averaging the usual Debye–Scherrer pattern was recorded. A similar construction was used for the small-angle regime, where a ring pattern was observed to grow in time. This light scattering apparatus was described in more detail before [23]. Due to technical reasons we performed the BLS and SALS measurements subsequently on each sample.

Before each measurement, the sample was slowly rotated for some hours to destroy any crystalline order. Abortion of shear and insertion of the sample into the experiment defines $t = 0$ min. A single measurement (one rotation of the detector arms with a stepper motor and detection of the scattered intensity in about 6000 steps) lasted about 30 s. Since the crystallization process occurred on times scales of hours to days it could be monitored with high temporal resolution.

Results

BLS results

BLS detects the time- and q-dependent scattered intensity, $I(q, t)$, on the length scale of the interparticle distances. Here $q = (4\pi n_S/\lambda_0)\sin(\theta/2)$ is the magnitude of the scattering vector, with n_S being the refractive index of the solvent, λ_0 the laser wavelength and θ the scattering angle. For better statistical accuracy, we summed up the scattered intensity over the whole ring. To correct for the form factor, $P(q)$, of the particles and the slightly different sensitivities of our photodiodes, we divided $I(q, t)$ by the intensity, $I(q, t = 0 \text{ min})$, at which only the shear molten state was present in the sample. We are aware that this procedure is somewhat problematic since we not only divide by $P(q)$, but also by other contributions, such as scattering from the remaining fluid. Further, after the appearance of crystallites an additional background may be present. In particular, completely random stacking may lead to a very pronounced broadening of selected peaks, thus affecting neighbouring reflections [22]. We note that more accurate correction procedures than the ones used here are available. For details see Refs. [7, 24].

In Fig. 3 the normalized scattering intensity, $I(q, t)/I(q, 0)$, for three selected times from $t = 10$ min up to $t = 3380$ min shows different growing Bragg peaks. They can be indexed {111}, {200}, {220}, {311} and {222} using the Miller indices of a fcc structure. We note that in the full two-dimensional scattering both {111} and {311} showed a sixfold symmetric scattering pattern superimposed on a ring pattern. This has been observed before in HS systems and originates from the presence of wall-nucleated, shear-oriented crystals [24]. The kinetics measured on angular-averaged data of both peaks shows two contributions and is not easy to interpret. Further, a distortion in the vicinity of the {111} reflection is present, probably due to the division by the fluid structure factor. {200} and {222} are very weak in comparison to the other peaks. {200}, which is expected to occur for a pure fcc lattice only, in particular may be subject to stacking-fault broadening and may contribute a nonnegligible background to the interlayer {111} reflection. Its weakness in the present case indicates a considerable degree of random stacking present in our sample at early times.

For these reasons we refrained from further evaluating {111}, {200}, {311} and {222}. In contrast, the fluid background at the position of the {220} reflection can be well approximated by a straight line [24] and no significant additional background due to random stacking or contributions from wall crystals should be present at this position. To isolate the peak we chose two limiting q values, q_1 and q_2, and subtracted a linear

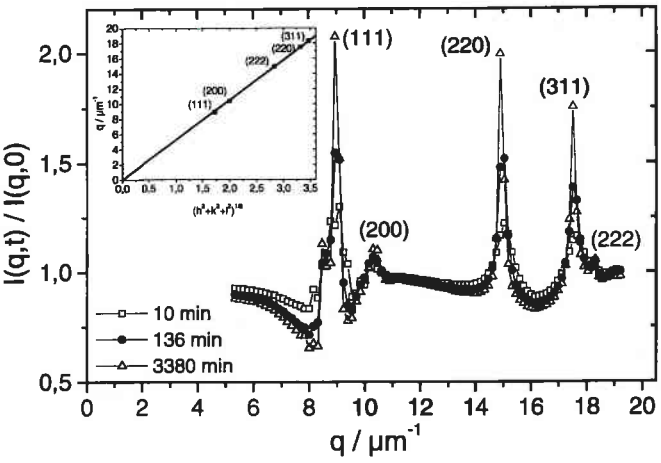

Fig. 3 Temporal evolution of the Bragg light scattering signal normalized as $I(q, t)/I(q, 0)$ for $t = 10$ min (□), 136 min (●) and 3380 min (△). The indexing uses Miller indices and the insert shows a face-centred-cubic structure to be present

function $I_U(q, t)$ through $I(q_1, t)$ and $I(q_2, t)$, resulting in the structure factor in the vicinity of the reflection:

$$S_{220}(q,t) = \frac{I(q,t)}{I(q,t=0)} - I_U(q,t) \ . \qquad (1)$$

The result for selected times covering more than 3 orders of magnitude is shown in Fig. 4. From $S_{220}(q, t)$ the area under the peak, $A_{220}(t)$, the full width at half maximum, $\Delta q_{220}(t)$, and the position of the maximum, $q_{220}(t)$, can be determined. An increase in $A_{220}(t)$ indicates an increase in the amount of crystalline material through both nucleation and growth. We fitted a Lorentzian function to $S_{220}(q, t)$ and integrated it between q_1 and q_2. We note that there is no meaning behind this choice other than a convenient parameterization of our data. A decrease in $\Delta q_{220}(t)$ indicates increasing crystal sizes. In fact, we may further calculate the radii, $R_C(t)$, from

$$R_C(t) = \frac{2\pi K}{\Delta q_{220}(t)} \ , \qquad (2)$$

with the constant $K = 1.107$ resulting from the assumption of crystallites of spherical shape [25].

The results for $A_{220}(t)$ and $R_C(t)$ are shown in Fig. 5 in a log-log plot. $A_{220}(t)$ shows a steep increase only at short times up to 10 min and then remains constant up to the longest times investigated. Since $A_{220}(t)$ is proportional to the crystallized volume in the sample, our data seem to indicate that after 10 min the processes of nucleation and growth have already finished and that the sample has completely solidified. On the other hand, $R_C(t)$ increases continuously. $R_C(t)$ is well described by a single power law of t^{α}, with $\alpha \approx 0.28$, until $t \approx 400$ min. Note that for our microgel particles, no transition regime is visible in $R_C(t)$ at $t = 10$ min. This is markedly

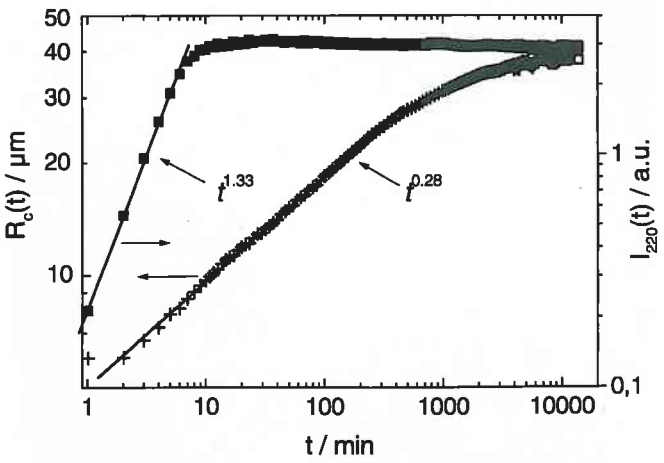

Fig. 5 *Upper curve, right scale*: integrated intensity $A_{220}(t)$ (■); *lower curve, left scale*: crystal size $R_C(t)$ (+), determined from the width of the reflection. *Solid lines*: fits using indicated power laws

different to previously investigated HS systems, where saturation in $A(t)$ corresponded to a change in the power law for $R_C(t)$, indicating the transition from nucleation and growth to ripening [7, 8].

Finally shifts in the peak position indicated compression or expansion of the crystal lattice. The results for $q_{220}(t)$ are shown in Fig. 6. We observed a shift in the peak position towards smaller scattering vectors in time. This is known from previous work on HS systems [7]. It has been interpreted as a slow expansion of crystallites from an initially compressed state. We calculated the corresponding crystal density decrease to obtain

$$\frac{\varphi_C(t=0) - \varphi_C(t \to \infty)}{\varphi_C(t \to \infty)} \approx 6\% \ . \qquad (3)$$

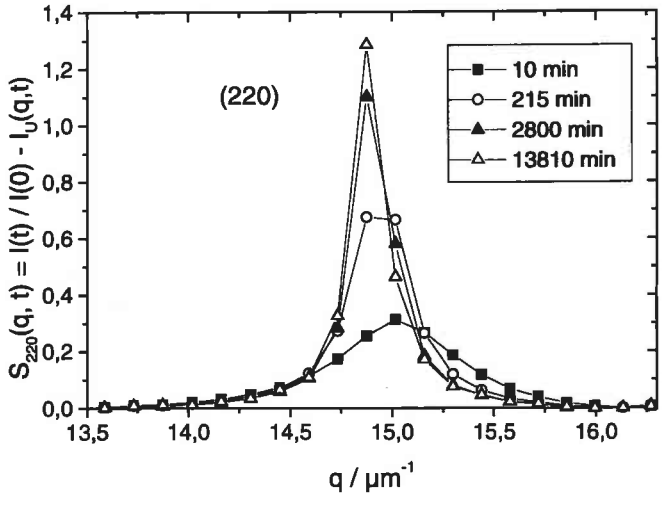

Fig. 4 Temporal evolution of the background-corrected intensity $I(t)/I(0) - I_U(q, t)$ of the {220} reflection for $t = 10$ min (■), 215 min (○), 2800 min (▲) and 13810 min (△)

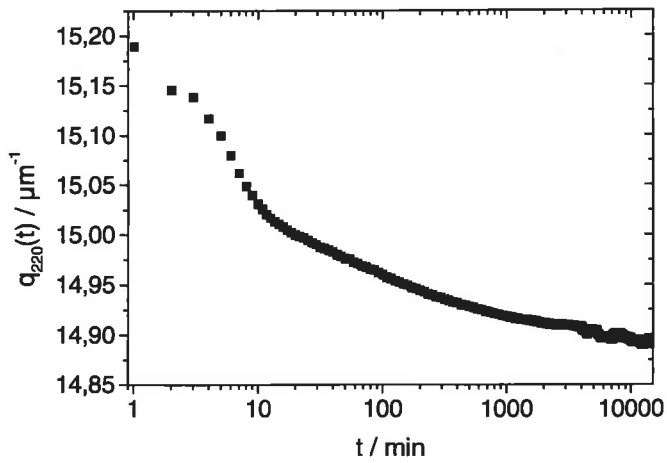

Fig. 6 Position of the maximum of the {220} reflection $q_{220}(t)$ versus time

This is in good agreement with the results in Ref. [7]. We note that while a change in the temporal behaviour of $q_{220}(t)$ seems to be present around $t = 10$ min, the data could not be fitted by power laws or other simple functions and thus no quantitative assertion can be given here.

SALS results

The SALS intensity was observed to remain practically constant, or even to slightly decrease, until $t_i \approx 100$ min. After this time a strong ringlike scattering signal i.e. a small-angle peak with a maximum at nonzero wave vector, evolves. To correct for stray light at small scattering vectors we followed Schätzel and Ackerson [8] and He et al. [9] and subtracted an early measurement from all the following measurements. We chose a correction time of $t = 93$ min, just before the peak appeared. The corrected small-angle intensity was then calculated as $I_{SA}(q, t) = I(q, t) - I(q, 93 \text{ min})$. The corrected data are shown in Fig. 7. The peak gains intensity and its maximum shifts towards smaller q.

Long induction times for SALS patterns have been reported before by van Duijneveldt [26]. For a system of slightly charged colloidal silica spheres with added electrolyte he reported t_i to vary between 610 and 2800 s. This was attributed to the formation of crystals with critical size, which then can grow further. Since our samples are already completely solidified at $t = 10$ min, we can rule out this explanation. Ring patterns have also been observed for HS systems of PMMA particles [8, 9]. They were interpreted as the "form factor" of growing crystals surrounded by a depletion zone of lower density and immersed in the shear molten fluid; however, there the patterns were already observed during nucleation and growth. Note that here the SALS pattern appears

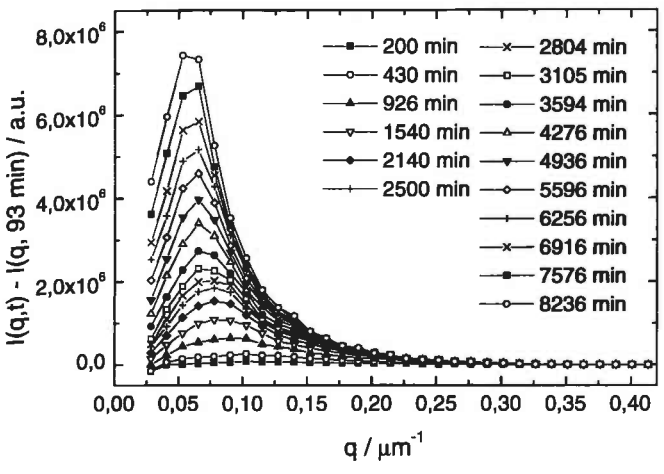

Fig. 7 Corrected small-angle data $I(q, t) - I(q, 93 \text{ min})$ for $t =$ 200 min (*lowest curve*) to $t = 8236$ min (*uppermost curve*)

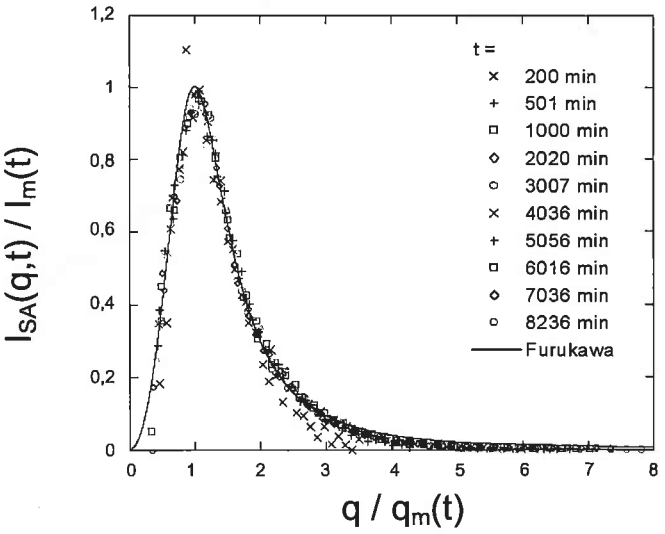

Fig. 8 Scaled small-angle light scattering data. The *solid line* is a plot of the Furukawa function calculated for $\delta = 3.0$

for times significantly longer than 10 min. This indicates a different scattering mechanism is present for our system.

To analyse the time dependence and check for scaling laws we plotted $I_{SA}(q, t)/I_m(t)$ versus $q/q_m(t)$. Here I_m is the intensity at the position of the maximum q_m. All the data collapse nearly on one single curve for times longer than 200 min. This is shown for times up to 8236 min in Fig. 8. Scaling has been observed before, but rarely over the whole range of times $t > t_i$ [9].

We tried to find a suitable scaling function $P(Q)$ with $Q = q/q_m$, such that the following relation holds:

$$I_{SA}(q,t) = I_m(t)\, P[q/q_m(t)] \quad . \tag{4}$$

Schätzel and Ackerson [8] used the function $P(Q) = 27Q^2/(2 + Q^2)^3$ to describe their data on PMMA HS. This function does not fit our data. Instead, we found the well-known Furukawa function [27] described the data well for intermediate and late times:

$$P(Q) = \frac{(1 + \delta/2)Q^2}{\delta/2 + Q^{\delta+2}} \quad . \tag{5}$$

The Furukawa function is known to apply to late-stage spinodal decomposition after off-critical quenches. It may be regarded as an interpolation between the limits $P(q) \sim q^2$ for small q and $P(q) \sim q^{-\delta}$ for large q. δ is related to the fractal dimension, d_f, of the scattering objects by $\delta = d_f + 1$. From the visual inspection of the sample at late times (Fig. 3) we first assumed compact and homogeneous scattering objects of smooth surface ($\delta = 4.0$). This does not describe our data. However, using $\delta = 3.0$ the solid curve in Fig. 8 results. As can be seen only for times up to $t \approx 200$ min there are visible

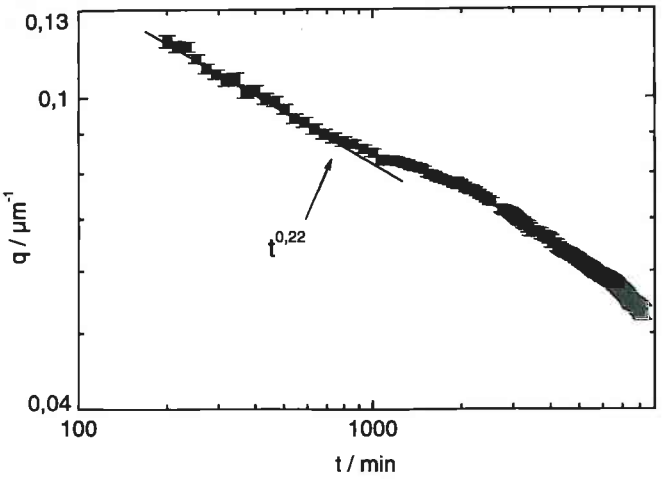

Fig. 9 Position of the small-angle peak $q_m(t)$ versus time. The fitted *solid line* indicates a $t^{0.22}$ behaviour for the first 1000 min

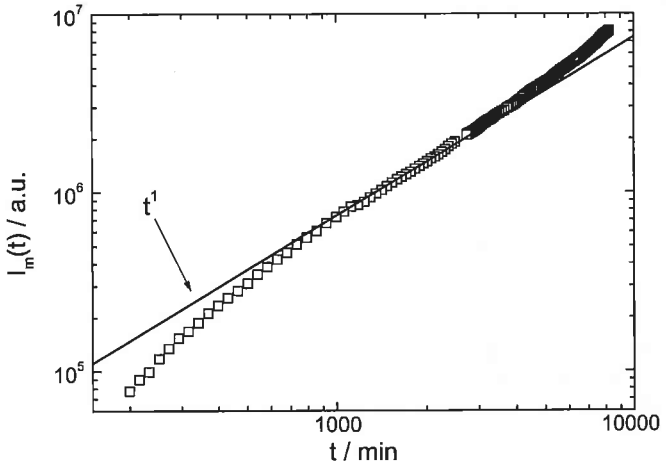

Fig. 10 Intensity of the small-angle peak $I_m(t)$ versus time. The *solid line* for comparison indicates a linear time law

deviations and the data fall slightly below the Furukawa curve.

The series of fits yield nearly identical values for δ, which slightly decreases from 3.2 for $t = 200$ min to about 2.7 for $t \geq 2000$ min. It is interesting to note that van Duijneveldt [26] found even smaller values of the large q exponent of 1.8–2.9. He suggests the form factors of fractal or highly asymmetric scattering objects as an explanation. It is not clear how to explain the deviation from Porod behaviour in our case.

The time evolution of $q_m(t)$ and $I_m(t)$ is shown in log-log plots in Figs. 9 and 10, respectively. $q_m(t)$ decreases in the first 1000 min with the power law $q_m(t) \sim t^{0.22}$. We conclude that the typical dimension of the objects giving rise to the SALS also increases with the same power law. Note that $\alpha = 0.22$ is very close to the exponent observed for $R_C(t)$ of 0.28. After a transition regime of slightly lower exponent the same or even a larger exponent is observed. $I_m(t)$ shows a continuous increase which is only approximately described by a power law. For comparison, the solid line shows a linear increase in $I_m(t)$ with time. Agreement is best around $t \approx 2000$ min. Deviations towards larger exponents are clearly visible for early and late times. Both exponents seem to show related temporal behaviour. The correspondence between the two exponents, however, remains unclear.

Discussion

We have investigated the crystallization kinetics in a sample of 1:10 cross-linked polystyrene microgel particles by combined SALS and BLS. Like in samples of HS colloids, we identified an early period of nucleation and growth, which is followed by a ripening region. The structure of the resulting solids was identified to be stacking-faulted fcc. The lattice constants show a slight increase indicating an expansion of the growing or ripening crystals. Further, a SALS peak could be observed to grow in time and shift towards smaller values of q, indicating sample inhomogeneity on length scales comparable to the crystal size. Relevant derived quantities could be shown to follow power-law behaviour for both BLS and SLS. In all these features our microgel samples very much resemble the behaviour known from crystallizing HS systems [3, 6–9, 19, 24–26] and are quite different to low-volume-fraction charged-sphere suspensions [10].

Most notably, however there are also specific differences. First of all, the SALS peak appears only after completed solidification. This rules out depletion zone scattering as a possible origin. Further, the values of the power-law exponents for $R_C(t)$ and $q_m(t)$ are nearly identical, indicating the possibility of SALS originating from the crystals alone; however, we are not aware of any form factor of crystallites giving rise to a maximum at finite q. Finally, this is the first time that Furukawa scaling was observed to hold for practically the whole range of times and scattering vectors; however, the value of $\delta = 3$ obtained would indicate two-dimensional objects as possible scattering objects. We therefore conclude that the origin of SALS is not identified in our case.

Also concerning the growth mechanism there seem to be marked differences. For BLS the crystallite size does not show any change in power law at the completion time of $t = 10$ min. This is in contrast to observations on HS, where nearly always a significant change in growth exponents occurred upon mutual touching of the crystallites or in depletion zones. Furthermore, the exponents of the power laws in our case are much

smaller than those reported before both for BLS and for SLS. The crystal-size-growth exponent, for example, is even slightly lower than that expected theoretically for Ostwald ripening ($\alpha = 1/3$). The mechanistic origin of such behaviour is not understood.

Our data pose a number of fundamental questions for the possibilities and mechanisms of solidification via crystallization in soft condensed matter systems. They clearly show that microgel colloids behave quite, but not completely, unlike crystallizing HS systems. Further research is clearly needed to clarify why these differences to HS systems appear, while the short-range ordered states are much more alike.

Acknowledgements We gratefully acknowledge the financial support of the following institutions: the Deutsche Forschungsgemeinschaft (DFG: Pa459/6-3), the Materialwissenschaftliches Forschungszentrum Mainz and the Sonderforschungsbereich SFB 262, Mainz.

References

1. Phan SE, Russel WB, Cheng Z, Zhu J, Chaikin PM, Dunsmuir JH, Ottewill RH (1996) Phys Rev E 54:6633
2. Vrij A (1983) Faraday Discuss Chem Soc 76:19
3. Pusey PN, van Megen W (1986) Nature 320:340
4. Hoover WG, Ree FH (1968) J Chem Phys 27:1208
5. Bartlett P, van Megen W (1994) In: Mehta A (ed) Granular matter. Springer, Berlin Heidelberg New York, pp 195–257
6. Palberg T (1997) Curr Opin Colloid Interface Sci 2:607
7. Harland JL, Henderson SI, Underwood SM, van Megen W (1996) Phys Rev Lett 75:3572
8. Schätzel K, Ackerson BJ (1992) Phys Rev E 48:3766
9. He Y, Ackerson BJ, van Megen W, Underwood SM, Schätzel K (1996) Phys Rev E 54:5286
10. Palberg T (1999) J Phys Condens Matter 11:R323
11. Saunders BR, Vincent B (1999) Adv Colloid Interface Sci 80:1
12. Bartsch E, Kirsch S, Lindner P, Scherer T, Stölken S (1998) Ber Bunsenges Phys Chem 102:1597
13. Bartsch E (1995) In: Yip E (ed) Relaxation kinetics in supercooled liquids – mode coupling theory and its experimental test, Transport Theory and Statistical Physics 24:1125
14. Bartsch E, Frenz V, Baschnagel J, Schärtl W, Sillescu H (1997) J Chem Phys 106:3743
15. Kasper A, Kirsch S, Renth F, Bartsch E, Sillescu H (1996) Prog Colloid Polym Sci 100:151
16. Kasper A, Bartsch E, Sillescu H (1998) Langmuir 14:5004
17. Kirsch S, Doerk A, Bartsch E, Sillescu H, Landfester K, Spiess HW, Maechtle W (1999) Macromolecules 32:4508
18. Kirsch S (1996) Ph D thesis. Mainz
19. Henderson SI, Mortensen TC, Underwood SM, van Megen W (1996) Physica A 233:102
20. Monovaukas Y, Gast A (1990) Phase Transitions 21:217
21. Elliot MS, Bristol BTF, Poon WCK (1997) Physica A 235:216
22. Pusey PN, van Megen W, Bartlett P, Ackerson BJ, Rarity JG, Underwood SM (1989) Phys Rev Lett 63:2753
23. Schätzel K (1996) In: Arora AK, Tata BVR (eds) Ordering and phase transitions in charged colloids. VCH, New York, pp 17–40
24. Heymann A, Stipp A, Sinn C, Palberg T (1998) J Colloid Interface Sci 206:119
25. Heymann A (1997) Ph D thesis. Mainz
26. van Duijneveldt JS (1994) PhD thesis. Utrecht
27. Furukawa H (1984) Physica A123:497